Theor Chem Acc (2011) 128:317–325
DOI 10.1007/s00214-010-0848-x

REGULAR ARTICLE

Theoretical studies and rate constants calculation for the reactions of acetone with fluorine and bromine atoms

Hui Zhang · Gui-ling Zhang · Jing-yao Liu · Miao Sun · Bo Liu · Ze-sheng Li

Received: 24 March 2010 / Accepted: 27 October 2010 / Published online: 13 November 2010

Abstract Theoretical investigations are carried out on the multichannel reactions $CH_3COCH_3 + F$ (R1) and $CH_3COCH_3 + Br$ (R2) by means of direct dynamics methods. The minimum energy path (MEP) is obtained at the MP2/6-31 + G(d,p) level, and energetic information is further refined at the MC-QCISD (single-point) level. The rate constants are calculated by the improved canonical variational transition-state theory (ICVT) with the small-curvature tunneling (SCT) contributions in a wide temperature range 200–1,500 K for the title reactions, H-abstraction channel is favored for the two reactions. The theoretical overall rate constants are in good agreement with the available experimental data and are found to be $k_{1a} = 3.22 \times 10^{-15} T^{1.51}\exp(1{,}190.91/T)$ cm^3 molecule^{-1} s^{-1}, $k_2 = 5.95 \times 10^{-18} T^{1.98}\exp(-4{,}622.45/T)$ cm^3 molecule^{-1} s^{-1}. Furthermore, the rate constants of reaction $Cl + CH_3COCH_3$ (R3) calculated in the other paper are added to discuss the reactivity trend of different halogen reaction with acetone on the rate constants of this class of hydrogen abstraction reactions.

Keywords Gas-phase reaction · Transition state · Rate constants

Electronic supplementary material The online version of this article (doi:10.1007/s00214-010-0848-x) contains supplementary material, which is available to authorized users.

H. Zhang · G. Zhang · M. Sun · B. Liu (✉)
College of Chemical and Environmental Engineering, Harbin University of Science and Technology, Harbin 150080, People's Republic of China
e-mail: hust_zhanghui1@hotmail.com

J. Liu
Institute of Theoretical Chemistry, Jilin University, Changchun 130023, People's Republic of China

Z. Li (✉)
Academy of Fundamental and Interdisciplinary Sciences, Department of Chemistry, Harbin Institute of Technology, Harbin 150080, People's Republic of China
e-mail: zeshengli@hit.edu.cn

Z. Li
School of Sciences, Beijing Institute of Technology, Beijng 100081, People's Republic of China

1 Introduction

Acetone is the simplest form of ketone. It represents an important class of oxygenated volatile organic compounds (VOCs) used widely as industrial solvents which fraction can escape into the atmosphere during use. Acetone reacts with various free radicals (e.g., OH, H, O, F, Cl, Br, etc.), which plays an important role in both atmospheric and combustion chemistry [1]. The degradation and accumulation of acetone in the upper troposphere and lower stratosphere has been highlighted [2–5]. Furthermore, in the dry regions of the upper troposphere, acetone can provide a large primary source of HO*x* (OH and HO_2) radicals, resulting in an increased ozone production. The surprisingly significant contribution of these oxygenated hydrocarbons to tropospheric HO*x* and ozone cycling is likely to be affected by natural and anthropogenic emission alterations due to the land-use changing, biomass burning as well as alcohol-based biofuel using. Herein, we investigated the mechanism and the accurate kinetics of the title reactions computationally by using high-level ab initio quantum chemistry methods.

The kinetic and mechanistic information available for the title reactions have been investigated in five previous works [6–10]. In 2001, the mechanism of reaction F atom

with acetone have been investigated by Nielsen O. J. and co-workers [6] using a FTIR-smog chamber system, and the results shown that the reaction of F + CH_3COCH_3 do not proceed solely via H atom abstraction, but rather a second channel involving a displacement mechanism is also involved. In 1977, the relative rate measurement of this reaction reported by Smith D. J. and co-workers [7] in a flowing-afterglow apparatus at room temperature, and the rate constant could be deduced as $(10 \pm 1) \times 10^{-11}$ cm^3 $molecule^{-1}$ s^{-1} at 295 K for H-abstraction channel. In 2005, the reaction F with acetone has been studied theoretically by Li and co-workers [8], the potential energy surface was calculated at G3MP2//MP2/6-311G(d,p) level, multichannel RRKM theory was employed to calculate the rate constants, and a negative temperature dependence of the overall rate constants was predicted at temperatures below 500 K. For the Br + CH_3COCH_3 reaction, King D. K. and co-worker [9] investigated the gas-phase thermal bromination of acetone over the temperature range 494—618 K, an extrapolation of the rate constant expression are given, the value of the rate constant was $(1.05 \pm 1.19) \times 10^{-20}$ cm^3 $molecule^{-1}$ s^{-1} at 298 K. In 2005, the relative-rate method coupled with gas chromatographic product analysis was employed to obtain the rate constants by Farkas E. and co-worker [10], the rate constant expression of the reaction is related to Br + *neo*-C_5H_{12} reaction in the temperature range 688–775 K, and the value of the converted of reaction Br atom with acetone was $(4.53 \pm 2.84) \times 10^{-20}$ cm^3 $molecule^{-1}$ s^{-1} at 298 K. Branching ratios of the reaction were not given in the literature. Three alternative reaction channels a, b, and c for each reaction have been investigated in this paper. The title reactions can proceed through H-abstraction from the CH_3 groups, halogen displacement for CH_3, and CH_3-abstraction from the acetone, along with the reaction R3 of Cl + CH_3COCH_3 investigated in other paper [11], i.e.,

$$\begin{aligned}
F + CH_3COCH_3 &\rightarrow CH_2COCH_3 + HF \ (R1a)\\
&\rightarrow CH_3C(O)FCH_3 \rightarrow CH_3COF\\
&\quad + CH_3 \ (R1b1 \text{ and } R1b2)\\
&\rightarrow CH_3CO + CH_3F \ (R1c)\\
Br + CH_3COCH_3 &\rightarrow CH_2COCH_3 + HBr \ (R2a)\\
&\rightarrow CH_3COBr + CH_3 (R2b)\\
&\rightarrow CH_3CO + CH_3Br \ (R2c)\\
Cl + CH_3COCH_3 &\rightarrow CH_2COCH_3 + HCl \ (R3a)\\
&\rightarrow CH_3COCl + CH_3 \ (R3b)\\
&\rightarrow CH_3CO + CH_3Cl \ (R3c)
\end{aligned}$$

Because the temperature used in the experiment is mostly at the lower end of the temperature range of practical interest, theoretical investigation is desirable to give a further understanding of the reaction mechanism of the multiple channel reactions and to evaluate the rate constant at high temperatures. To our best knowledge, no other previous work has addressed these reactions.

In order to obtain more reliable results for the rate constants of the title reactions and branching ratio in the reaction R2 over a wide temperature range 200–1,500 K, dual-level direct dynamics methods [12–16] are employed in the present study. The potential energy surface information, including geometries, energies, gradients, and force constants of the stationary points (reactant, complexes, products, and transition states) and 16 extra points along the minimum energy path (MEP), is obtained directly from electronic structure calculations. Subsequently, by means of POLYRATE 9.1 program [17], the rate constants are calculated by using the variational transition-state theory (VTST) proposed by Truhlar and co-workers [18, 19]. The comparison between theoretical and experimental results is discussed.

2 Computational method

In the present work, the equilibrium geometries and frequencies of all the stationary points are optimized at the restricted or unrestricted second-order Møller-Plesset perturbation (MP2) [20–22] level with the 6-31+G(d,p) basis set. Molecular electrostatic potentials [23] of CH_3COCH_3, F, Cl, and Br atoms are calculated at the same level and plotted using gOpenMol 2.32 [24]. The MEP is obtained by intrinsic reaction coordinate (IRC) theory in mass-weighted Cartesian coordinates with a gradient step-size of 0.05 $(amu)^{1/2}$ bohr. At the same level, the energy derivatives, including gradients and Hessians at geometries along the MEP, are obtained to calculate the curvature of the reaction path and the generalized vibrational frequencies along the reaction path. Furthermore, the energy profile is refined by multi-coefficient correlation method based on quadratic configuration interaction with single and double excitations MC-QCISD [25] based on the MP2/6-31+G(d,p) geometries. All electronic structure calculations are performed by means of GAUSSIAN03 program package [26].

VTST [18, 19] is employed to calculate the rate constants by the POLYRATE 9.1 program [17]. The improved canonical variational transition-state theory (ICVT) [27] incorporating small-curvature tunneling (SCT) [28, 29] contributions proposed by Truhlar and co-workers [19, 30] is applied to evaluate the theoretical rate constants. For the title reaction, all vibrational modes are treated as quantum–mechanical separable harmonic oscillators except for the lowest vibrational mode that is treated by using the hindered rotor model [22, 23]. The hindered rotor approximation of Truhlar and Chuang [31, 32] is used for calculating the partition function of these modes. The

curvature components are calculated using a quadratic fit to obtain the derivative of the gradient with respect to the reaction coordinate.

3 Results and discussions

3.1 Stationary points

The optimized geometric parameters of the reactant (CH_3COCH_3), complexes (CR1aR, CR1aF, and CR1b2R), products (CH_3COCH_2, HF, CH_3COF, CH_3, CH_3CO, CH_3F, HBr, CH_3COBr, and CH_3Br), and transition states (TS1a, TS1b1, TS1b2, TS1c, TS2a, TS2b, and TS2c) for seven reaction channels (R1a, R1b1, R1b2, R1c, R2a, R2b, and R2c) calculated at the MP2/6-31+G(d,p) level are presented in Fig. 1 along with the available experimental data [33, 34]. It can be seen that the theoretical geometric parameters of CH_3COCH_3, HF, HBr, CH_3, CH_3F, and CH_3Br are in good agreement with the corresponding experimental values [33, 34]. Furthermore, two complexes (CR1aR and CR1aF) are presented on the reactants and products sides of reaction R1a. At the MP2/6-31+G(d,p) level, the H···F and O···H bonds distance in CR1aR and CR1aF are 3.29 and 1.62 Å, respectively. The other complex CR1b2R is located on the reactants sides of reaction R1b, at the MP2/6-31+G(d,p) level, the C···F bond distance in CR1bR is 1.42 Å. For the transition states TS1a and TS1c, the lengths of C–H and C–C bond, which will be broken, are stretch by 4 and 14% compared to the regular lengths of C–H and C–C bond in CH_3COCH_3, and the forming H–F and C–F bonds are elongated by about 55 and 30% over the equilibrium bond length in isolated HF and CH_3F, respectively. The elongation of the breaking bond is smaller than that of the forming bond, indicating that TS1a and TS1c are all reactant-like, i.e., the two reaction channels will proceed via "early" transition states, consistent with Hammond's postulate [35], applied to for an exothermic hydrogen abstraction reaction. On the other hand, in the structures of TS2a, TS2b, and TS2c, the C–H and C–C bonds, which will be broken, are stretched by 44, 30, and 33% compared with the equilibrium bond lengths in isolated CH_3COCH_3, respectively; and the forming bonds H–Br and C–Br are elongated by 7, 5, and 16% with respect to the equilibrium bond lengths of the molecules HBr, CH_3COBr, and CH_3Br, respectively. The results imply that the barriers of reactions R2a, R2b, and R2c are both near the corresponding products, and consequently, both of them will proceed via "late" transition states, as expected for an endothermic reaction.

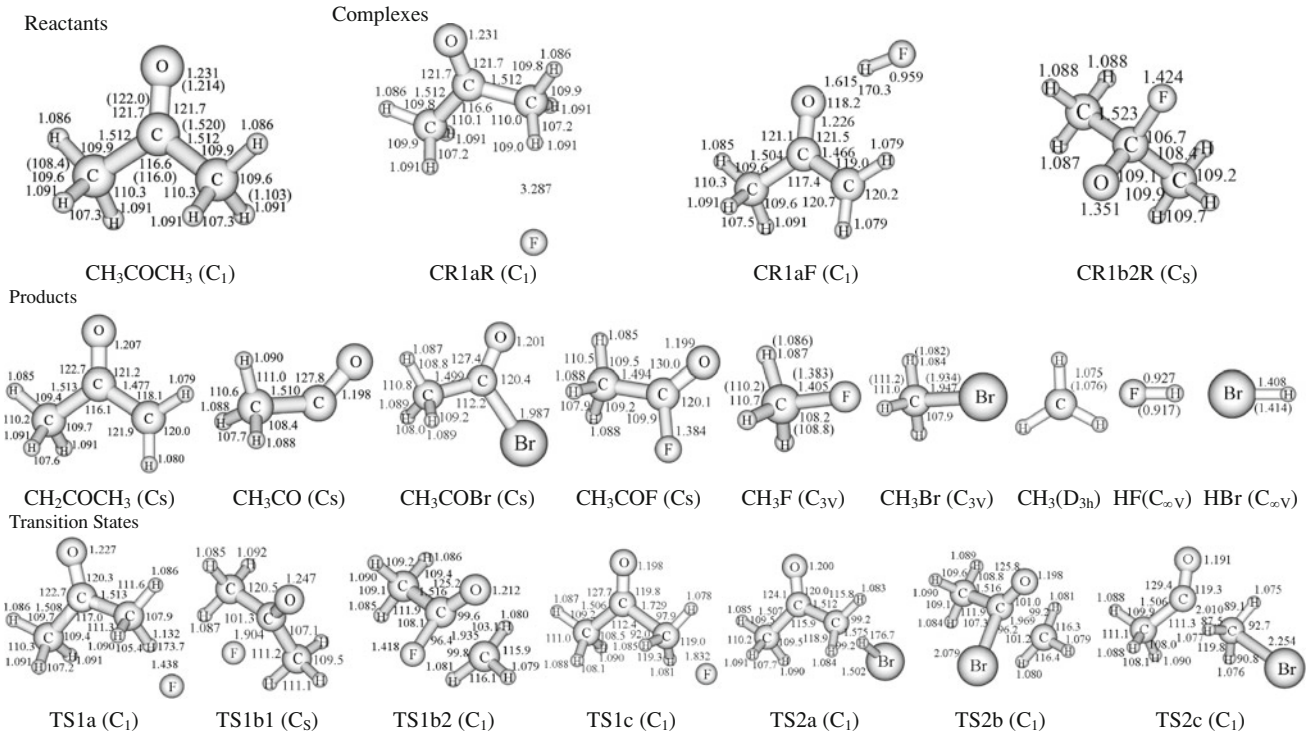

Fig. 1 Optimized geometries of the reactant, complexes, products, and transition states at the MP2/6-31 + G(d,p) level. The values in parentheses are the experimental values (ref 33 for CH_3COCH_3, CH_3F, CH_3Br, and CH_3, ref 34 for HF and HBr). Bond lengths are in angstroms, and angles are in degrees

Table 1 Calculated and experimental frequencies (cm^{-1}) for the reactant, complexes, products, and transition states for the title reaction at the MP2/6-31 + G(d,p) level

Species	MP2/6-31 + G(d,p)	Expt.
CH_3COCH_3	3255, 3254, 3208, 3203, 3121, 3117, 1762, 1529, 1518, 1510, 1509, 1435, 1430, 1278, 1139, 1108, 925, 909, 815, 536, 488, 384, 125, 48	3019,[a] 2972, 2963, 2937, 1731, 1454, 1435, 1426, 1410, 1364, 1216, 1091, 1066, 891, 877, 777, 530, 484, 385
CH_2COCH_3	3392, 3270, 3256, 3125, 3125, 2094, 1516, 1514, 1502, 1430, 1292, 1098, 1056, 918, 832, 638, 538, 521, 388, 230, 81	
HF	4119	
HBr	2733	2649[b]
CH_3CO	3242, 3236, 3122, 1939, 1506, 1505, 1406, 1083, 981, 899, 471, 74	1875,[a] 1420
CH_3COBr	3260, 3240, 3136, 1840, 1509, 1507, 1431, 1137, 1063, 982, 573, 501, 342, 308, 137	3017,[c] 1817, 1417, 1367, 1083, 950, 567, 500
CH_3COF	3279, 3242, 3148, 1894, 1521, 1519, 1448, 1212, 1089, 1029, 826, 586, 566, 416, 132	3043,[a] 3004, 2955, 1870, 1440, 1437, 1378, 1188, 1054, 1000, 826, 598, 567, 420, 123
CH_3	3430, 3430, 3232, 1478, 1478, 469	3171,[d] 3004, 1403
CH_3F	3260, 3260, 3144, 1551, 1551, 1525, 1213, 1213, 1057	3006,[a] 1467, 1464, 1182, 1049
CH_3Br	3297, 3297, 3169, 1524, 1524, 1397, 1007, 1007, 630	3056,[a] 2972, 1443, 1306, 955, 611
CR1aR	3255, 3254, 3209, 3204, 3122, 3116, 1761, 1529, 1517, 1508, 1494, 1432, 1431, 1276, 1140, 1109, 924, 907, 815, 536, 488, 385, 131, 29, 20, 19, 17	
CR1aF	3423, 3395, 3274, 3259, 3216, 3127, 2012, 1521, 1513, 1506, 1440, 1332, 1108, 1053, 954, 942, 877, 854, 683, 564, 535, 402, 265, 227, 91, 66, 49	
CR1b2R	3259, 3255, 3253, 3252, 3143, 3142, 1547, 1537, 1525, 1520, 1449, 1427, 1272, 1221, 1218, 995, 992, 973, 924, 779, 531, 461, 437, 324, 317, 263, 223	
TS1a	3269, 3259, 3212, 3170, 3123, 1933, 1744, 1520, 1512, 1465, 1435, 1369, 1351, 1222, 1130, 1084, 913, 893, 808, 529, 484, 371, 172, 116, 59, 33, 698*i*	
TS1b1	3279, 3277, 3233, 3227, 3134, 3129, 1637, 1531, 1512, 1502, 1499, 1443, 1431, 1301, 1117, 1079, 970, 897, 827, 532, 467, 408, 277, 205, 184, 118, 812*i*	
TS1b2	3386, 3372, 3276, 3239, 3188, 3135, 1818, 1523, 1518, 1490, 1473, 1426, 1165, 1111, 1030, 955, 744, 709, 555, 494, 352, 307, 281, 260, 234, 213, 637*i*	
TS1c	3364, 3310, 3265, 3237, 3137, 3133, 1891, 1513, 1509, 1459, 1420, 1418, 1211, 1164, 1147, 1052, 1002, 930, 558, 499, 373, 320, 177, 131, 118, 78, 1657*i*	
TS2a	3343, 3271, 3218, 3213, 3125, 2359, 1517, 1511, 1484, 1431, 1324, 1249, 1115, 1058, 897, 815, 736, 681, 616, 532, 521, 388, 328, 117, 76, 36, 591*i*	
TS2b	3382, 3368, 3279, 3250, 3188, 3146, 1733, 1528, 1525, 1493, 1474, 1436, 1178, 1154, 1035, 989, 779, 762, 721, 564, 523, 417, 281, 269, 240, 171, 773*i*	
TS2c	3422, 3403, 3253, 3237, 3205, 3128, 2025, 1507, 1501, 1440, 1431, 1410, 1164, 1145, 1118, 1047, 1000, 904, 502, 457, 333, 204, 186, 126, 92, 63, 844*i*	

[a] Ref. [36], [b] Ref. [37], [c] Ref. [38], [d] Ref. [39]

Table 1 lists the harmonic vibrational frequencies of all the stationary points involved the reactant, complexes, products, and transition states at the MP2/6-31 + G(d,p) level as well as the corresponding available experimental results [36–39]. The seven transition states in Table 1 are confirmed by normal-mode analysis to have only one imaginary frequency corresponding to the stretching modes of the coupling between breaking and forming bonds. The values of those imaginary frequencies are 698*i* cm^{-1} for reaction R1a, 812*i* cm^{-1} for reaction R1b1, 637*i* cm^{-1} for reaction R1b2, 1,657*i* cm^{-1} for reaction R1c, 591*i* cm^{-1} for reaction R2a, 773*i* cm^{-1} for reaction R2b, and 844*i* cm^{-1} for reaction R2c.

3.2 Energetics

The reaction enthalpies at 298 K (ΔH^0_{298}), for reactions R1a, R1b2, R1c, R2a, R2b, R2c, R3a, R3b, and R3c calculated at the MC-QCISD//MP2/6-31+G(d,p) level are listed in Table 2, as well as the available experimental reaction enthalpies [37, 38, 40, 41]. The reaction enthalpies are single point energies which are refined at MC-QCISD level based on the MP2/6-31+G(d,p) geometries. It is shown that the three individual reactions R2a, R2b, and R2c are all endothermic reaction, consistent with the discussion above of Hammond's postulate [35]. The calculated reaction enthalpies are in good agreement with the corresponding experimental values, which were derived from the standard heats of formation (F, 18.96 kcal/mol [37]; Cl, 28.97 kcal/mol [37]; Br, 26.72 kcal/mol [37]; CH_3COCH_3, −51.69 kcal/mol [40]; CH_2COCH_3, −8.61 kcal/mol [37]; HF, −65.10 kcal/mol [37]; HCl, −22.05 kcal/mol [37]; HBr, −8.70 kcal/mol [37]; CH_3CO, −2.87 ± 0.72 kcal/mol [38]; CH_3COF, −106.29 ± 0.48 kcal/mol [41]; CH_3COBr, −46.81 ± 0.72 kcal/mol [41]; CH_3F, −55.96 kcal/mol [37]; CH_3Cl, −19.99 kcal/mol [37]; CH_3Br, −9.08 ± 0.31 kcal/mol [37]; CH_3, 34.80 kcal/mol [37]). In the other paper [11], the rate constants of reaction Cl + CH_3COCH_3 (R3) have been calculated at BMC-CCSD//MP2/6-31+G(d,p) level. In present work, the reactivity trend of different halogen (F, Cl, and Br) reaction with acetone on the rate constants will be discussed. While the BMC-CCSD method (mlgauss2.0) did not including basis function of Br atom, the energies cannot be calculated using BMC-CCSD method for reaction R2. So the reaction enthalpies for the reaction channels R1a, R1b2, R1c, R3a, R3b, and R3c are calculated at BMC-CCSD//MP2/6-31+G(d,p) level. The corresponding values are also listed in the Table 2. The values calculated at various levels agree well with each other. So the values calculated at MC-QCISD//MP2/6-31+G(d,p) level are expected to be reliable. Thus, in the present study, we use MC-QCISD//MP2/6-31+G(d,p) method to calculate the potential energy barriers as well as the energies along the MEP in the following studies.

A schematic potential energy surface of the reactions F + CH_3COCH_3 and Br + CH_3COCH_3 obtained at the MC-QCISD//MP2/6-31+G(d,p) + ZPE level is described in Fig. 2. Note that the energies of reactants are set to be zero for reference. At MC-QCISD//MP2/6-31+G(d,p) level, for the reaction R1b1, F is found to add to

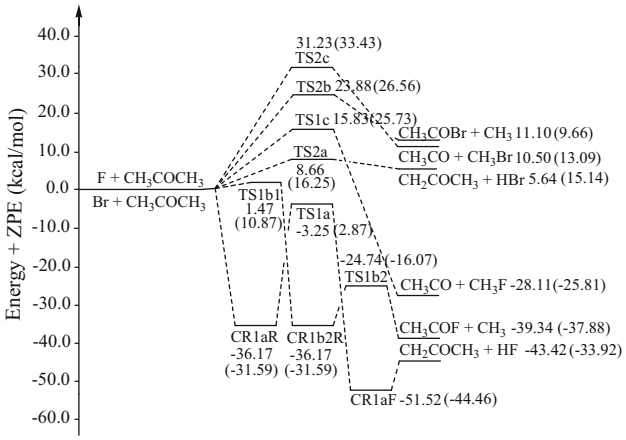

Fig. 2 Schematic potential energy surface for F + CH_3COCH_3 and Br + CH_3COCH_3 reactions. Relative energies (in unit of kcal/mol) are calculated at the MC-QCISD//MP2/6-31 + G(d,p) + ZPE level and the MP2/6-31 + G(d,p) + ZPE level (the values in *parentheses*)

Table 2 The reaction enthalpies at 298 K (ΔH^0_{298}) (kcal/mol) for the reactions of F, Cl, and Br atoms with CH_3COCH_3 at the MC-QCISD//MP2/6-31 + G(d,p) and BMC-CCSD//MP2/6-31 + G(d,p) levels together with the experimental values

	MC-QCISD//MP2	BMC-CCSD//MP2	Expt.
ΔH^0_{298}			
F + CH_3COCH_3 → CH_2COCH_3 + HF (R1a)	−42.9	−40.7	−41.0
F + CH_3COCH_3 → $CH_3C(O)FCH_3$ (R1b1)	−37.5	−37.2	
F + CH_3COCH_3 → CH_3COF + CH_3 (R1b)	−39.0	−37.8	−38.8 ± 0.5
F + CH_3COCH_3 → CH_3CO + CH_3F (R1c)	−28.0	−26.1	−26.1 ± 0.7
Cl + CH_3COCH_3 → CH_2COCH_3 + HCl (R3a)	−7.6	−7.0	−7.9
Cl + CH_3COCH_3 → CH_3COCl + CH_3 (R3b)	−0.9	−0.2	−2.5 ± 0.1
Cl + CH_3COCH_3 → CH_3CO + CH_3Cl (R3c)	0.1	0.8	−0.1 ± 0.7
Br + CH_3COCH_3 → CH_2COCH_3 + HBr (R2a)	6.1		7.7
Br + CH_3COCH_3 → CH_3COBr + CH_3 (R2b)	11.8		13.0 ± 0.7
Br + CH_3COCH_3 → CH_3CO + CH_3Br (R2c)	10.7		13.0 ± 0.7

Experimental value derived from the standard heats of formation: F, 18.96 kcal/mol [37]; Cl, 28.97 kcal/mol [37]; Br, 26.72 kcal/mol [37]; CH_3COCH_3, −51.69 kcal/mol [40]; CH_2COCH_3, −8.61 kcal/mol [37]; HF, −65.10 kcal/mol [37]; HCl, −22.05 kcal/mol [37]; HBr, −8.70 kcal/mol [37]; CH_3CO, −2.87 ± 0.72 kcal/mol [38]; CH_3COF, −106.29 ± 0.48 kcal/mol [41]; CH_3COBr, −46.81 ± 0.72 kcal/mol [41]; CH_3F, −55.96 kcal/mol [37]; CH_3Cl, −19.99 kcal/mol [37]; CH_3Br, −9.08 ± 0.31 kcal/mol [37]; CH_3, 34.80 kcal/mol [37]

CH_3COCH_3 forming $CH_3C(O)FCH_3$ (similarity with a reaction of acetone + OH [42]); there is a barrier of 1.47 kcal/mol with ZPE corrections. This addition path has not been mentioned on the reference of theoretical studied by Yuzhen L. and co-workers [8]. For the reaction R1b2, one complex (CR1b2R) with the relative energy 36.17 kcal/mol lower than the reactants F + CH_3COCH_3 is found on the reactants side, the barrier of TS1b2 taking the value of −24.74 kcal/mol at the MC-QCISD//MP2 level, that is consistent with the literature reports [8]. At the same time, for reaction R1a, the attack of F atom on the C–H bond of CH_3COCH_3 would proceed via a complex (CR1aF) on the products side, which is 8.10 kcal/mol lower than the corresponding products, and a complex (CR1aR) on the reactants side, which is 36.17 kcal/mol lower than the reactants. For reaction channel R1a, at the MP2/6-31+G(d,p) level, the barrier for TS1a is 2.87 kcal/mol. However, this barrier is reduced significantly to be negative (−3.25 kcal/mol) at the higher MC-QCISD level. This implies that the H-abstraction reaction channel is actually a barrierless process. The barrier of TS1a taking the value of −3.25 kcal/mol at the MC-QCISD//MP2 level is about 19.1 kcal/mol lower than that of TS1c, which indicates that H-abstraction channel is more favorable than the CH_3-abstraction channel. At the same time, reaction R1a is more exothermic than reaction R1b by about 15.3 kcal/mol. On the basis of above calculation, reaction R1a is more favorable than reaction R1c both thermodynamically and kinetically, while the CH_3-abstraction channel may be negligible. For reaction acetone with Br atom, the potential barrier heights are 8.66 kcal/mol for reaction R2a, 23.88 kcal/mol for reaction R2b, and 31.23 kcal/mol for reaction R2c at MC-QCISD//MP2/6-31 + G(d,p) + ZPE level; the former reaction path R2a is less endothermic than the later R2b and R2c by about 5.5 and 4.9 kcal/mol, respectively, and as a result, the reaction channel reaction R2a is more thermodynamically and kinetically favorable than the later R2b and R2c. Thus, we infer that reaction channel R2a is the dominant channel for the reaction CH_3COCH_3 + Br. H-abstraction channel (R2a) is expected to be the major one with larger rate constants, and the Br-displacement (R2b) and CH_3-abstraction channel (R2c) are minor pathways.

3.3 Rate constants

Theoretical calculations rate constants of the reaction F + CH_3COCH_3 → CH_3COCH_2 + HF and Br + CH_3COCH_3 → products are carried out at the MC-QCISD//MP2/6-31+G(d,p) level. The rate constants of the individual channel, k_{1a} for R1a, k_{2a} for R2a, k_{2b} for R2b, and k_{2c} for R2c are evaluated by conventional transition state theory (TST) and the ICVT in a wide temperature range from 200 to 1,500 K. Tunneling effect is included by means of the SCT contributions. The calculated TST, ICVT, and ICVT/SCT rate constants of the three reaction channels for reaction R2 are plotted against the reciprocal of temperature in Fig. 3, and also given in Table S1 as supplementary information. The calculated TST, ICVT, and ICVT/SCT rate constants of the reaction channels R1a are given in Table S2 as supplementary information together with the overall ICVT/SCT rate constants k_2 for reaction R2, k_3 for reaction R3, and corresponding experimental value [7–10, 43–50]. The TST, ICVT, and ICVT/SCT rate constants k_{1b1} of the reaction channel R1b1 and k_{1c} for reaction R1c are given in Table S3 as supplementary information together with the overall ICVT/SCT rate constants k_1. Note that the variational effects, i.e., the ratio between ICVT and TST rate constants, are important in the lower temperature range for reactions R1a and R2a. The ratios of k_{1a}(ICVT)/k_{1a}(TST) are 0.48, 0.40, and 0.34 at 200, 400, and 600 K, respectively. The ratios of k_{2a}(ICVT)/k_{2a}(TST) are 0.21, 0.44, and 0.52 at 200, 400, and 600 K, respectively. For reactions R2b and R2c, ICVT and TST rate constants are nearly the same over the whole temperature range, which indicates that the variational effects are almost negligible. On the other hand, considering the tunneling effect of the three reaction channels for reaction R2, i.e., the ratio between ICVT/SCT and ICVT rate constants, plays an important role at the lower temperatures and is negligible at high temperatures. For example, the ratios of k(ICVT/SCT)/k(ICVT) are 4.99, 3.90, and 28.5 at 200 K for R2a, R2b, and R2c, respectively, while they are 1.22, 1.17, and 1.35 at 600 K, respectively. For reaction R1a, the tunneling effect is small; the ratios of k_{1a}(ICVT/SCT)/k_{1a}(ICVT) are 0.84, 0.76, and 0.74 at 200, 400, and 600 K, respectively.

Figure 3 shows that the rate constants of reactions R2a, k_{2a}, are about 3–16 and 2–21 orders of magnitude higher

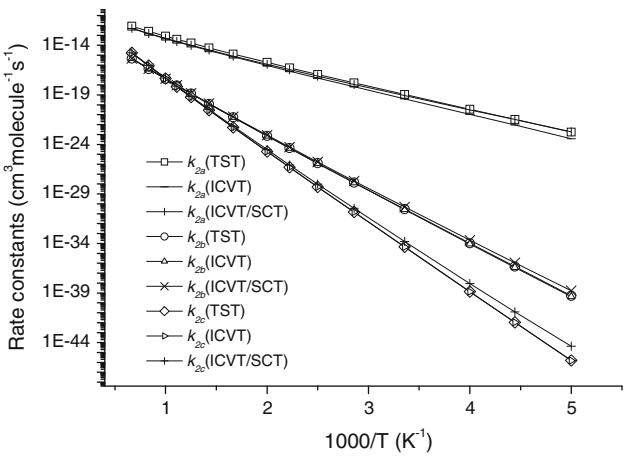

Fig. 3 The TST, ICVT, and ICVT/SCT rate constants (in cm^3molecule^{-1} s^{-1}) calculated at the MC-QCISD//MP2/6-31 + G(d,p) level for three reaction channels, k_{2a} for R2a, k_{2b} for R2b, and k_{2c} for R2c, versus 1,000/T between 200 and 1,500 K

than those of reaction R2b and R2c, k_{2b} and k_{2c}, from 200 to 1500 K, respectively. It can be concluded that the H-abstraction channel from the CH_3 group is always absolutely dominant in the temperature range 200–1,500 K, and Br-displacement and CH_3-abstraction channels from the CH_3COCH_3 are minor pathways. This is consistent with a qualitative assessment based on the potential energy barrier heights and the reaction enthalpies of these reaction channels.

The overall theoretical ICVT/SCT rate constants k_2 and k_3 are calculated from the sum of the corresponding individual rate constants, i.e., $k_2 = k_{2a} + k_{2b} + k_{2c}$, $k_3 = k_{3a} + k_{3b} + k_{3c}$, which are displayed in Fig. 4 along with the theoretical ICVT/SCT rate constants k_{1a} and the corresponding experimental data [7–10, 43–50]. The anti-Arrhenius behavior of k_{1a} could be clearly seen from the auxiliary small figure in the Fig. 4. The theoretical ICVT/SCT rate constants of k_3 at 298 K, 2.34×10^{-12} cm^3 molecule^{-1} s^{-1}, are in good agreement with the available experimental values [43–50], and the ratio of $k_{ICVT/SCT}$/kexptl remains within a factor of approximately 0.76-1.38. For Br + CH_3COCH_3 reaction with the theoretical ICVT/SCT rate constants of k_2 at 298 K, 8.39×10^{-20} cm^3 molecule^{-1} s^{-1}, experimental rate constants was determined by King D. K. and co-worker [9] over the temperature range 494—618 K, the value was given as $(1.05 \pm 1.19) \times 10^{-20}$ cm^3 molecule^{-1} s^{-1} at 298 K. The value investigated is related to Br + *neo*-C_5H_{12} reaction in the temperature range 688–775 K, and the converted was given as $(4.53 \pm 2.84) \times 10^{-20}$ cm^3 molecule^{-1} s^{-1} by Farkas E. and co-worker [10]. The theoretical ICVT/SCT rate constants of k_{1a} at 295 K, 1.02×10^{-10} cm^3 molecule^{-1} s^{-1}, are in good agreement with the available experimental value $(10 \pm 1) \times 10^{-11}$ cm^3 molecule^{-1} s^{-1} at 295 K [7] and the result of the theoretically calculated by Yuzhen L. and co-workers 9.8×10^{-11} cm^3 molecule^{-1} s^{-1} at 295 K [8].

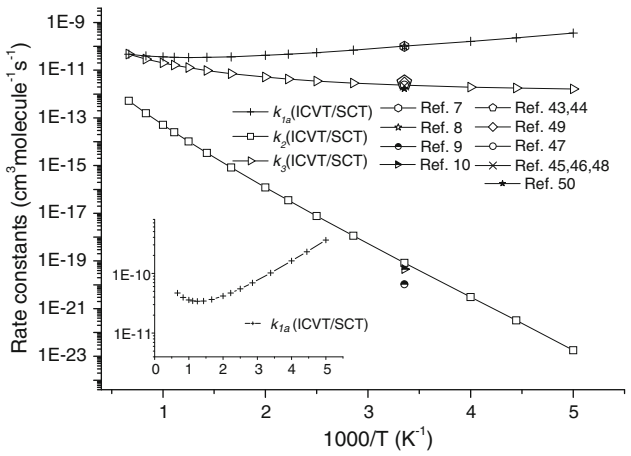

Fig. 4 The ICVT/SCT rate constants calculated at the MC-QCISD//MP2/6-31 + G(d,p) level for F + CH_3COCH_3 (k_{1a}), Br + CH_3COCH_3 (k_2), and Cl + CH_3COCH_3 (k_3) (in cm^3 molecule^{-1} s^{-1}) versus 1,000/T between 200 and 1,500 K together with the corresponding experimental values [7–10, 43–50]

As a result of the limited experimental knowledge of the kinetics of the title reaction, we hope that our present study may provide useful information for further laboratory investigations. For convenience of future experimental measurements, three-parameter fits of the ICVT/SCT rate constants of R1a, three reaction channels of reaction R2, and the overall rate constants of reaction R2 in the temperature range 200–1,500 K are performed, and the expressions are given as follows (in unit of cm^3 molecule^{-1} s^{-1}):

$$k_{1a}(T) = 3.22 \times 10^{-15} T^{1.51} \exp(1190.91/T)$$

$$k_{2a}(T) = 6.13 \times 10^{-18} T^{1.97} \exp(-4624.03/T)$$

$$k_{2b}(T) = 1.01 \times 10^{-20} T^{2.51} \exp(-11306.24/T)$$

$$k_{2c}(T) = 1.35 \times 10^{-21} T^{3.25} \exp(-14319.45/T)$$

$$k_2(T) = 5.95 \times 10^{-18} T^{1.98} \exp(-4622.45/T).$$

3.4 Reactivity trends

The difference of the rate constants of reactions of halogen (F, Cl, and Br) with CH_3COCH_3 can be qualitatively illustrated by the different energy levels of the highest occupied molecular orbital (HOMO) of CH_3COCH_3 and halogen (F, Cl, and Br). The HOMO of halogen is singly occupied and could accept partial electron from CH_3COCH_3. The results of theoretical calculations at the MP2/6-31+G(d,p) level show that with the increasing periodic number, the HOMO energies of F (−0.73 hartree), Cl (−0.50 hartree), and Br (−0.46 hartree) gradually increase. While the HOMO energy of CH_3COCH_3 (−0.42 hartree) is 0.31, 0.08, and 0.04 hartree higher than F, Cl, and Br ones, respectively, the LOMO energy of CH_3COCH_3 is 0.07 hartree. For the three reactions, the HOMO orbit joins the reaction of halogen, but the higher virtual molecule orbit than LOMO joins the reaction for the CH_3COCH_3 molecule. As a result, the reactions of halogen with CH_3COCH_3 are exothermic once, and the value of exothermic of the reaction F + CH_3COCH_3 is the maximum, so the reaction rate is the fastest. This means that for the above-mentioned three reactions, with the n increase for the attack atoms F, Cl, Br, the reaction rate constants decrease in the order of F + CH_3COCH_3 > Cl + CH_3COCH_3 > Br + CH_3COCH_3. This is consistent with a qualitative assessment based on the potential energy barrier heights by the present work and the previous experimental investigation [7–10, 43–50].

The molecular electrostatic potential is an important tool to analyze molecular reactivity because it can provide the information about local polarity. Figure 5 gives the distribution of the molecular electrostatic potential. There, the

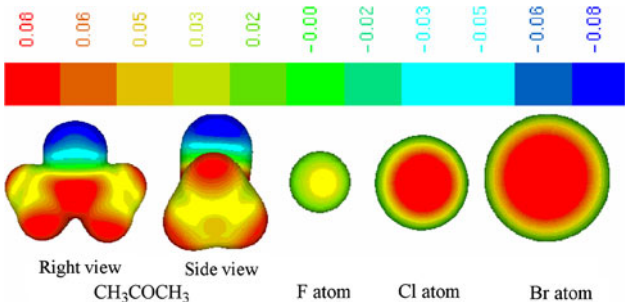

Fig. 5 The calculated electrostatic potential textured vDW surfaces for the reactants

most negative and positive potentials are assigned to be blue and red, respectively, and the color spectrum is mapped to all other values by linear interpolation. The more positive potential region (more red) will be more favored for the halogen to attack at. It is found that in molecule CH_3COCH_3, the H atoms bear stronger positive potential (red) than the C atoms of CH_3 groups (yellow), indicating that the H atoms can be more easily attacked by the halogen. Note that the halogen atom is encircled by marked negative potential; therefore, the halogen atom is more preferably to attack the H atom of CH_3COCH_3 comparing to the CH_3 group. From these results, we could infer that the H-abstraction reaction channel of CH_3COCH_3 with halogen could occur more easily than the CH_3-abstraction reaction. This is in line with the rate constant results calculated above.

4 Conclusions

In this paper, the reactions $F + CH_3COCH_3$ and $Br + CH_3COCH_3$ have been studied theoretically by means of direct dynamics methods. The potential energy surface information is obtained at the MP2/6-31+G(d,p) level, and higher-level energies for the stationary points and a few extra point along the minimum energy path are further refined by the MC-QCISD method. Three reaction channels are identified, one for H-abstraction from the CH_3 group, and the others for halogen displacement for CH_3 and CH_3-abstraction from the CH_3COCH_3 for the two reactions. The results of the theoretical investigation mean that for the three reactions, with the n increase for the attack atoms F, Cl, Br, the reaction rate constants decrease in the order of $F + CH_3COCH_3 > Cl + CH_3COCH_3 > Br + CH_3COCH_3$. For the three reactions, the calculated potential barriers show that major pathway is H-abstraction from the CH_3 group. At the MC-QCISD//MP2 level, the calculated ICVT/SCT rate constants, k_{1a}, k_2, and k_3, are in good agreement with the corresponding available temperature values, we expect that the theoretical results may be useful for estimating the kinetics of the reaction over a wide temperature range where no experimental data is available.

Acknowledgments The authors thank Professor Donald G. Truhlar for providing POLYRATE 9.1 program. This work is supported by the National Natural Science Foundation of China (20333050, 20303007, and 20973049), the Program for New Century Excellent Talents in University (NCET), the Doctor Foundation by the Ministry of Education, the Foundation for the Department of Education of Heilongjiang Province (1152G010, 11551077), the Key subject of Science and Technology by the Ministry of Education of China, the SF for Graduate Innovate by the Department of Education of Heilongjiang Province (YJSCX2009-055HLJ), and Natural Science Foundation of Heilongjiang Province (B200605).

References

1. Chatfield RB, Gardner EP, Calvert JG (1987) J Geophys Res 92:4208
2. Singh HB, O'Hara D, Herlth D, Sachse W, Blake DR, Bradshaw JD, Kanakidou M, Crutzen PJ (1994) J Geophys Res 99:1805
3. Singh HB, Kanakidou M, Crutzen PJ, Jacob DJ (1995) Nature 378:50
4. Arnold F, Knop G, Zierens H (1986) Nature 321:505
5. Arnold F, Burger V, Drost-Fanke B, Grimm F, Schneider J, Krieger A, Stile T (1997) Geophys Res Lett 24:3017
6. Nielsen OJ, Johnson MS, Wallington TJ, Christensen LK, Platz J (2001) Int J Chem Kinet 34:283
7. Smith DJ, Setser DW, Kim KC, Bogan DJ (1977) J Phys Chem 81:898
8. Li YZ, Li H, Hou H, Wang BS (2005) J Phys Chem A 109:3166
9. King DK, Golden DM, Benson SW (1970) J Am Chem Soc 92:5541
10. Farkas E, Kovács G, Szilágyi I, Dóbé S, Bérces T, Márta F (2001) Int J Chem Kinet 33:49
11. Zhang H, Zhang GL, Liu JY, Miao S, Liu B, Li ZS (2008) Theo Chem Acc 119:445–451
12. Bell RL, Truong TN (1994) J Chem Phys 101:10442
13. Truong TN, Duncan WT, Bell RL (1996) Chemical applications of density functional theory. American Chemical Society, Washington, DC, p 85
14. Truhlar DG (1995) The reaction path in chemistry: current approaches and perspectives, edited by Heidrich, D. Kluwer, Dordrecht, p 229
15. Corchado JC, Espinosa-Garcia J, Hu W-P, Rossi I, Truhlar DG (1995) J Phys Chem 99:687
16. Hu W-P, Truhlar DG (1996) J Am Chem Soc 118:860
17. Corchado JC, Chuang Y-Y, Fast PL, Villa J, Hu W-P, Liu Y-P, Lynch GC, Nguyen KA, Jackels CF, Melissas VS, Lynch BJ, Rossi I, Coitino EL, Ramos AF, Pu J, Albu TV (2002) POLYRATE version 9.1. Department of Chemistry and Supercomputer Institute, University of Minnesota, Minneapolis
18. Truhlar DG, Garrett BC (1980) Acc Chem Res 13:440
19. Truhlar DG, Isaacson AD, Garrett BC (1985) In: Baer M (ed) The theory of chemical reaction dynamics, vol 4. CRC Press, Boca Raton, p 65
20. Duncan WT, Truong TN (1995) J Chem Phys 103:9642
21. Frisch MJ, Head-Gordon M, Pople JA (1990) Chem Phys Lett 166:275
22. Head-Gordon M, Pople JA, Frisch MJ (1988) Chem Phys Lett 153:503

23. Boris B, Petia B (1999) J Phys Chem A 103:6793
24. Bergman DL, Laaksonen L, Laaksonen A (1997) J Mol Graphics Modell 15:301
25. Fast PL, Truhlar DG (2000) J Phys Chem A 104:6111
26. Frisch MJ, Trucks GW, Schlegel HB, Scuseria GE, Robb MA, Cheeseman JR, Montgomery JA Jr, Vreven T, Kudin KN, Burant JC, Millam JM, Iyengar SS, Tomasi J, Barone V, Mennucci B, Cossi M, Scalmani G, Rega N, Petersson GA, Nakatsuji H, Hada M, Ehara M, Toyota K, Fukuda R, Hasegawa J, Ishida M, Nakajima T, Honda Y, Kitao O, Nakai H, Klene M, Li X, Knox JE, Hratchian HP, Cross JB, Adamo C, Jaramillo J, Gomperts R, Stratmann RE, Yazyev O, Austin AJ, Cammi R, Pomelli C, Ochterski JW, Ayala PY, Morokuma K, Voth GA, Salvador P, Dannenberg JJ, Zakrzewski VG, Dapprich S, Daniels AD, Strain MC, Farkas O, Malick DK, Rabuck AD, Raghavachari K, Foresman JB, Ortiz JV, Cui Q, Baboul AG, Clifford S, Cioslowski J, Stefanov BB, Liu G, Liashenko A, Piskorz P, Komaromi I, Martin RL, Fox DJ, Keith T, Al-Laham MA, Peng CY, Nanayakkara A, Challacombe M, Gill PMW, Johnson B, Chen W, Wong MW, Gonzalez C, Pople JA (2003) Gaussian, Inc., Pittsburgh
27. Garrett BC, Truhlar DG, Grev RS, Magnuson AW (1980) J Phys Chem 84:1730
28. Lu DH, Truong TN, Melissas VS, Lynch GC, Liu YP, Grarrett BC, Steckler R, Issacson AD, Rai SN, Hancock GC, Lauderdale JG, Joseph T, Truhlar DG (1992) Comput Phys Commun 71:235
29. Liu Y-P, Lynch GC, Truong TN, Lu D-H, Truhlar DG, Garrett BC (1993) J Am Chem Soc 115:2408
30. Steckler R, Hu W-P, Liu Y-P, Lynch GC, Garrett BC, Isaacson BAD, Melissas VS, Lu D-P, Truong TN, Rai SN, Hancock GC, Lauderdale JG, Joseph T, Truhlar DG (1995) Comput Phys Commun 88:341
31. Truhlar DG (1991) J Comput Chem 12:266
32. Chuang YY, Truhlar DG (2000) J Chem Phys 112:1221
33. Kuchitsu K (ed) (1998) Structure of free polyatomic molecules basic data. Springer, Berlin, vol 1, p 156, 105, 104, 102
34. In NIST Chemistry WebBook, NIST Standard Reference Database Number 69, June 2005 Release. The date compiled by Huber K. P.; Herzberg, G.
35. Hammond GS (1955) J Am Chem Soc 77:334
36. In NIST Chemistry WebBook, NIST Standard Reference Database Number 69, June 2005 Release, Vibrational frequency (date compiled by Shimanouchi, T.)
37. Chase, M. W. (1998) NIST-JANAF themochemical tables, 4th edn. ACS, Washington, DC, J Phys Chem Ref Data Monogr 9:1–1951
38. In NIST Chemistry WebBook, NIST Standard Reference Database Number 69, June 2005 Release, Data compilation copyright by the U.S. Secretary of Commerce
39. In NIST Chemistry WebBook, NIST Standard Reference Database Number 69, June 2005 Release, Vibrational frequency (date compiled by Jacox, M. E.)
40. In NIST Chemistry WebBook, NIST Standard Reference Database Number 69, June 2005 Release, Date compiled by Stein, S.E.
41. In NIST Chemistry WebBook, NIST Standard Reference Database Number 69, June 2005 Release, Date compiled by Afeefy, H. Y.; Liebman, J. F.; Stein, S. E.
42. Masgrau L, González-Lafont À, Lluch JL (2002) J Phys Chem A 106:11760
43. Orlando JJ, Tyndall GS, Vereecken L, Peeters J (2000) J Phys Chem A 104:11578
44. Notario A, Mellouki A, Bras GL (2000) Int J Chem Kinet 32:62
45. Carr S, Shallcross DE, Canosa-Mas CE, Wenger JC, Sidebottom HW, Treacy JJ, Wayne RP (2003) Phys Chem Chem Phys 5:3874
46. Martínes E, Aranda A, Díaz-de-mera Y, Rodríguez A, Rodríguez D, Notario A (2004) J Atmos Chem 48:283
47. Wallington TJ, Andino JM, Ball JC, Japar SM (1990) J Atmos Chem 10:301
48. Christensen LK, Ball JC, Wallington TJ (2000) J Phys Chem A 104:345
49. Albaladejo J, Notario A, Cuevas CA, Ballesteros B, Martínez E (2003) J Atmos Chem 45:35
50. Olsson B, Hallquist M, Ljungström E, Davidsson J (1997) Int J Chem Kinet 29:195